Proceedings of the International Gas Turbine Congress 2003 Tokyo
November 2-7, 2003

IGTC2003Tokyo TS-064

Effects of Swirl and Flow Rate on the Flow and Heat Transfer in a Pre-swirl Rotating-disc System

Mahmood FARZANEH-GORD, Michael WILSON and J. Michael OWEN

Department of Mechanical Engineering
University of Bath
Bath BA2 7AY UK
Phone: +44-1225-386-325, FAX: +44-1225-386-928, E-mail: ensmw@bath.ac.uk

ABSTRACT

Pre-swirl is often used in the internal cooling-air systems of gas turbines to reduce the temperature of the cooling air relative to the rotating turbine blades. In a "direct-transfer" system, the air passes axially across the wheel-space from stationary pre-swirl nozzles to receiver holes in the rotating turbine disc. This paper investigates the effects of inlet flow conditions and rotational speed on the flow and heat transfer in such a system, using a simplified computational model for 3D steady, incompressible turbulent flow. Computed results are compared with measurements of tangential velocity and Nusselt number made in a complementary experimental study.

The results show that there are significant mixing losses near the inlet nozzles, resulting in a reduced “effective” pre-swirl ratio at inlet. The computed tangential velocity distributions suggest free-vortex-type behaviour for the flow between the pre-swirl nozzle radius and that of the receiver holes. There is mainly good agreement between the computed and measured velocities, although the measured values are generally lower than the computed values and follow free-vortex behaviour less closely. There is less good agreement between computed and measured values of Nusselt number, although the correct trends are obtained for the effects of the main flow parameters.

NOMENCLATURE

a , b	inner, outer radius of disc
c_p	specific heat of air at constant pressure
C_w	nondimensional mass flow rate (= $\dot{m}$ /μb)
d	pre-swirl nozzle diameter
G	gap ratio (= s/b)
k	turbulence kinetic energy, thermal conductivity of air
$\dot{m}$	mass flow rate
N	number of pre-swirl nozzles
Nu	local Nusselt number (=qr/k(T_{aw} – T_w))
Pr	Prandtl number (=μc_p /k)
q	heat flux (from air to disc)
r, ϕ, z	radial, tangential and axial coordinates
R	recovery factory (=$Pr^{1/3}$)
Re_ϕ	Rotational Reynolds number
s	axial spacing between stator (z=0) and rotor (z=s)
T	temperature
T_a	total temperature of pre-swirl air at inlet
T_w	temperature at rotor disc surface (wall)
U_τ	friction velocity (= $\sqrt{\tau_w / \rho}$)
V_r, V_ϕ, V_z	time-averaged radial, circumferential, axial components of velocity in stationary frame
x	nondimensional radius (= r/b)
y	distance normal to the wall
y+	nondimensional distance (= ρyU_τ/μ)
z	axial distance
β	swirl ratio (= V_ϕ /Ωr)
β_p	pre-swirl ratio (= $V_{\phi,p}$ /Ωr_p)
ε	turbulence energy dissipation rate
λ_T	turbulent flow parameter (= $C_{w,p}/Re_\phi^{0.8}$)
θ	angle of pre-swirl nozzle to tangential direction
μ	dynamic viscosity
ρ	density
τ_w	wall shear stress
Ω	angular speed of disc

Subscripts

aw	adiabatic wall value
b	blade-cooling air, at receiver hole radius
p	pre-swirl air, at pre-swirl nozzle radius
s	sealing air
∞	mid-plane z/s=0.5 (outside of boundary layers)

INTRODUCTION

Yan et al (2002) carried out measurements and three-dimensional computations for the flow structure in the idealised pre-swirl rotor-stator system shown schematically in Fig. 1, and Lock et al (2003) described an investigation of the heat transfer in the same system using a transient thermochromic liquid crystal (TLC) technique. The system shown in Fig. 1 models the pre-swirl chamber near the periphery of a rotating turbine disc and an adjacent stationary casing used in some gas-turbine engines. Air is introduced through discrete nozzles in the stator, angled in the direction of rotation of the disc, and enters receiver holes located at a higher radius on the rotating disc. In an engine, this air is used to cool the turbine blades, and the pre-swirl at inlet reduces the relative total temperature of the air entering the holes, see Owen and Rogers (1989).

The results obtained by Yan et al (2002) show that the flow in the pre-swirl system has some similarities with that found in classical rotor-stator systems. As illustrated in Fig. 2, computations show that there is a recirculating secondary flow, with radial outflow in the boundary layer on the rotating disc and radial inflow on the stator (outward of the pre-swirl nozzle centreline).

The measurements and computations made by Yan et al showed that significant losses in total pressure occurred between the inlet nozzles and the plane mid-way between the rotor and stator (where pitot-tube measurements were made). These mixing losses, which were caused by a momentum exchange between the primary pre-swirl flow and the recirculating secondary flow, increased as the inlet pre-swirl ratio β_p increased.

Manuscript Received on March 31, 2003

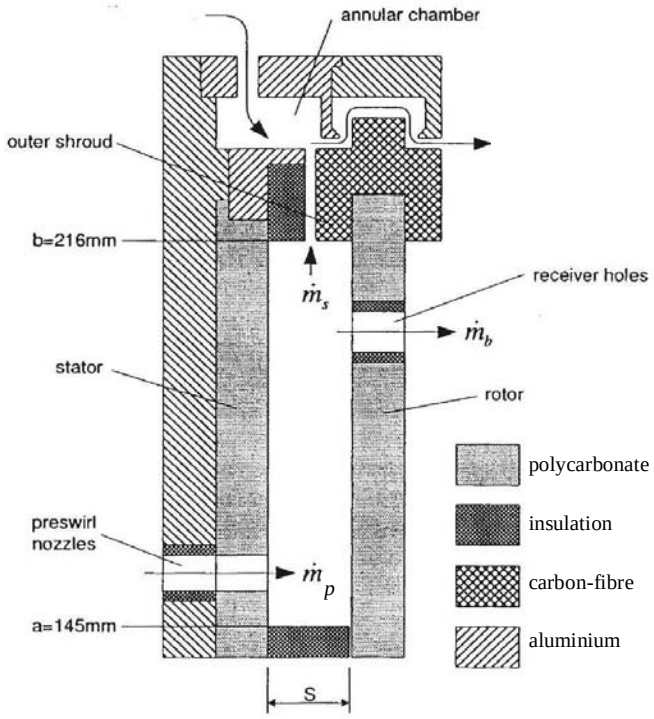

Fig. 1 Schematic diagram of experimental pre-swirl rig (Yan et al, 2002, not to scale)

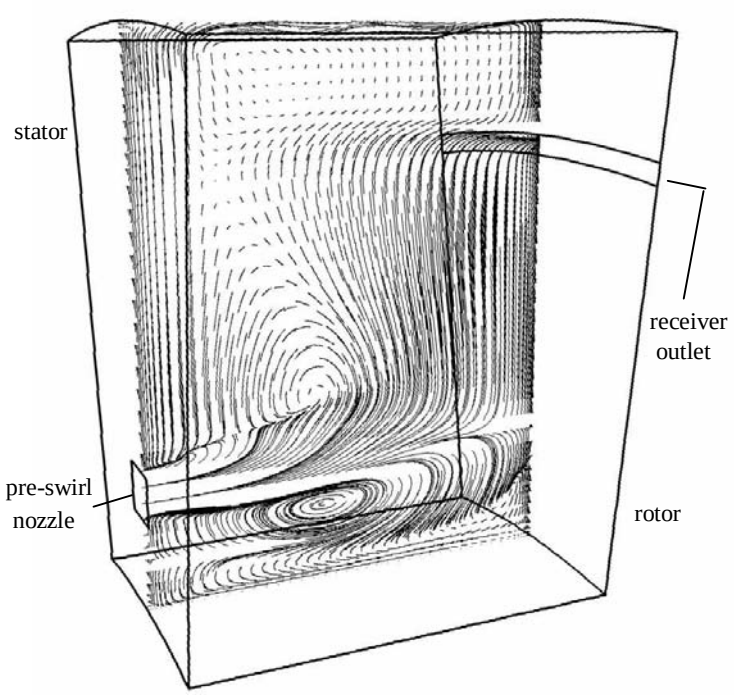

Fig. 2 Computed secondary flow structure

As found by Karabay et al and other research workers, Yan et al also concluded that the flow structure in the pre-swirl chamber is controlled principally by the pre-swirl ratio, β_p, and the turbulent flow parameter, $\lambda_T = C_w Re_\phi^{-0.8}$. (The turbulent flow parameter, which combines the effects of the nondimensional pre-swirl flow rate, C_w, and the rotational Reynolds number, Re_ϕ, for the disc, is related to the entrainment of fluid into the boundary layer on a rotating disc; for turbulent flow, $\lambda_T \approx 0.22$ for the entrainment due to an unconfined disc.) The present paper describes the flow structure in more detail, and discusses the effects of β_p, λ_T and Re_ϕ on the heat transfer between the air and the rotating disc.

Owen and Rogers (1989) described early work on pre-swirl systems, and Owen and Wilson (2002) gave a brief review of more recent heat transfer research. Much of this work concerned the temperature of the air entering the receiver holes; the present study is concerned mainly with the heat transfer at the disc surface.

Karabay et al (2001) carried out a combined experimental and computational study of flow in a "cover-plate" pre-swirl system. The cooling air from the stationary pre-swirl nozzles flowed radially outward (to the receiver holes) in a rotating cavity formed by the rotating disc and a cover-plate attached to it. Free vortex flow was found to occur for this system, and a theoretical analysis was used to show that there was an optimal value of the pre-swirl ratio, for which the average Nusselt number for a heated rotating disc would be a minimum.

Pilbrow et al (1999) presented experimental and computational results for heat transfer in the same cover-plate system. Local Nusselt numbers, Nu, for the heated disc were found to depend principally on Re_ϕ, λ_T and β_P. Nu increased with increasing Re_ϕ, and λ_T affected the shape of the Nu distribution; for low values of λ_T, non-entraining Ekman-type boundary layers formed on the co-rotating discs, giving rise to lower heat transfer rates than were measured (and computed) at higher values of λ_T. Axisymmetric computations, carried out using low-Reynolds-number k-ε turbulence models, were mostly in good agreement with the measured Nu and reproduced the parametric variations observed in the experiments. No heat transfer measurements were made for the lower part of the system (around the pre-swirl inlet nozzle radius), where the computations showed a local peak in Nu, suggesting impingement-like behaviour of the pre-swirl flow on the heated disc surface.

The 3D steady flow model used by Yan et al has been extended to make corresponding heat transfer predictions, and the further details of the model are given below. Computed and measured tangential velocity distributions are used to investigate free-vortex type behaviour in the system and the mixing losses near the pre-swirl inlets. Computed and measured distributions of Nu over the disc surface are presented, and the variation of Nu with λ_T and Re_ϕ is described for both the measured data and the computed results.

COMPUTATIONAL MODEL AND TEST CONDITIONS

Fig. 1 shows a schematic diagram of the experimental rig on which the computational model is based. Briefly, there are twenty-four discrete pre-swirl inlet nozzles on the stator, angled at 20° to the tangential direction, and sixty circular receiver holes on the rotating disc (the rotor). The non-dimensional centreline radius of the pre-swirl nozzles is $x_p = 0.74$, and that of the receiver holes is $x_b = 0.93$. The gap ratio is $G = s/b = 0.051$. (As illustrated in Fig. 1, a sealing flow could be drawn from the clearance between the rotating and stationary sections of the outer casing; the effect of the modest sealing flow rates tested was found to be small when compared with results obtained for cases without sealing flow.) Since the inlet nozzle angle is fixed, the pre-swirl ratio β_P varies with inlet flow rate, see Yan et al (2002). Higher values of pre-swirl ratio ($\beta_P > 1.5$) were obtained in experiments by reducing the number of nozzles, N, from 24 to 12 (by blocking every other nozzle). Heat transfer measurements for the rotating disc were obtained using an unheated disc and heated inlet pre-swirl air. Yan et al (2002) and Lock et al (2003) give more details of the rig and the experimental methods used. The parameter ranges covered experimentally were as follows:

$0.78 \times 10^6 < Re_\phi < 1.2 \times 10^6$

$0.6 \times 10^4 < C_w < 2.8 \times 10^4$ ($0.11 < \lambda_T < 0.36$)

$0.5 < \beta_p < 1.5$ (N = 24) and $1.0 < \beta_p < 3.0$ (N = 12)

The ranges of λ_T and β_p are typical of those used in practice. Whilst the maximum value of Re_ϕ is an order of magnitude smaller than that found in engines, the flow structures and trends in heat transfer described here are believed to be representative.

The computational model is that described by Yan et al and only brief details are given here, together with the additional details pertinent to heat transfer. The 3D steady incompressible-flow model involves one of the discrete pre-swirl nozzles on the stator of the experimental rig, with cyclic symmetry conditions applied at the tangential faces of the domain. In order to permit steady flow computations, an annular outlet is used on the rotor, as illustrated in Fig. 2. This outlet matches the centreline radius and total flow area of the sixty receiver holes. The low-Reynolds-number k-ε turbulence model of Launder and Sharma (1974) was used; constant fluid properties were assumed and a discretised equation for static temperature was solved assuming a Prandtl number Pr = 0.71 and a turbulent Prandtl number of 0.9. A 99 × 150 × 21 (axial × radial × tangential) grid was used for the N = 24 cases described here; for the N =12 cases, the tangential extent of the domain was doubled and the number of points in the tangential direction was increased by 10. Values of the non-dimensional distance y^+ were around unity for the near-wall grid point at all solid surfaces.

Computations were carried out for comparison with results from an extensive programme of experimental tests. Measurements of pre-swirl flow rate, $\dot{m}_p$, and inlet total temperature, T_a, were used to prescribe uniform boundary conditions for the inlet flow at the pre-swirl nozzle for individual cases. Typically, T_a was around 55 °C. A uniform axial velocity and (and zero radial velocity) were prescribed at the annular outlet on the rotor, in order to ensure global mass conservation. A zero normal-derivative condition was used at outlet for both tangential velocity and static temperature.

The local Nusselt number Nu is defined as:

$$Nu = \frac{qr}{k(T_w - T_{aw})} \qquad (1)$$

where:

$$T_{aw} = T_a + \frac{1}{2c_p}\left\{R(\Omega r - V_{\phi,\infty})^2 - V_{\phi,\infty}^2\right\} \qquad (2)$$

Eq. (2) for T_{aw} is based on the theoretical adiabatic-wall temperature given by Karabay et al (2001), although making use of the measured total temperature of the inlet air, T_a. The transient heat transfer experiments give rise to a time-varying distribution of temperature T_w over the unheated rotor; for the steady-state computations, the initial air temperature measured prior to the start of each transient test was used as the uniform disc temperature. (Studies suggest that computed Nu is not sensitive to the radial variations of temperature that occur with time in the experiments.) Temperatures on the stator, and on the inner and outer surfaces, were not measured in the experiments and adiabatic conditions were assumed for the computations.

FLUID DYNAMICS RESULTS

Swirl ratio and effective pre-swirl ratio

Yan et al (2002) showed comparisons between computed and measured variations of (tangentially-averaged) swirl ratio β_∞ ($=V_{\phi,\infty}/\Omega r$) with non-dimensional radius x (=r/b) along the mid-plane between the rotor and stator (z/s=0.5). Fig. 3 and Fig. 4 show further comparisons, for a range of test conditions, for N = 24 and N = 12 respectively but plotted against x^{-2} instead of against x. The technique of plotting β_∞ against x^{-2}, which was used by Karabay et al (2001), is described below.

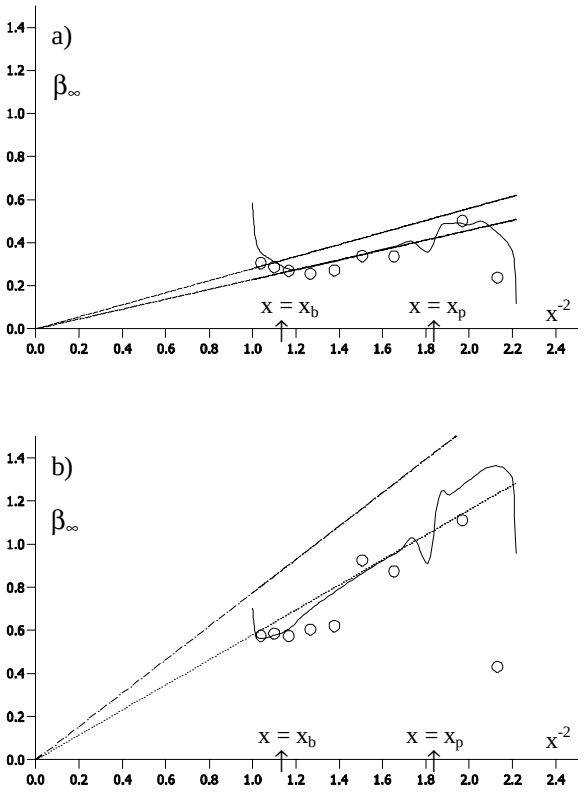

Fig. 3 Computed and measured radial variation of β_∞ for N=24
a) $Re_\phi = 0.80\times10^6$, $\lambda_T = 0.126$, $\beta_p = 0.51$
b) $Re_\phi = 0.78\times10^6$, $\lambda_T = 0.369$, $\beta_p = 1.49$
computed ——— , measured O
free vortex: ideal, Eq. (3) - - - - , effective, Eq. (4) .....

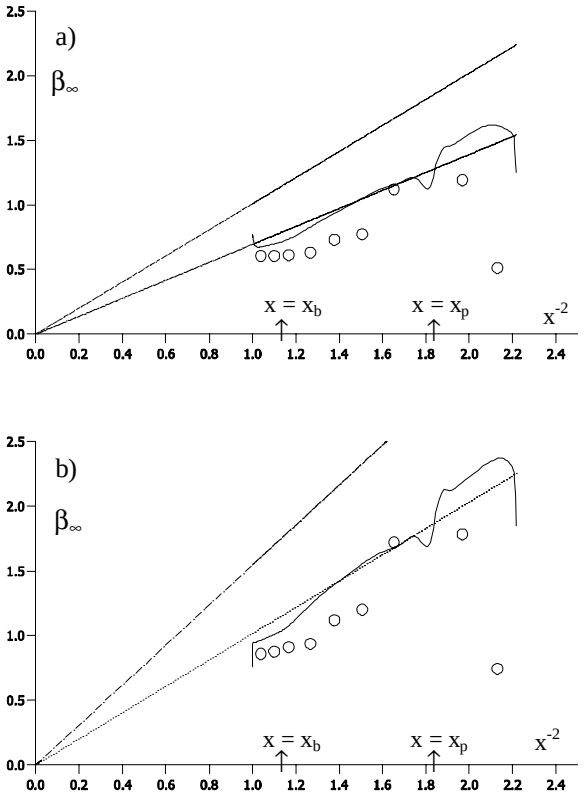

Fig. 4 Computed and measured radial variation of β_∞ for N=12
a) $Re_\phi = 1.18\times10^6$, $\lambda_T = 0.245$, $\beta_p = 1.84$
b) $Re_\phi = 0.79\times10^6$, $\lambda_T = 0.347$, $\beta_p = 2.82$
(for legend see Fig. 3)

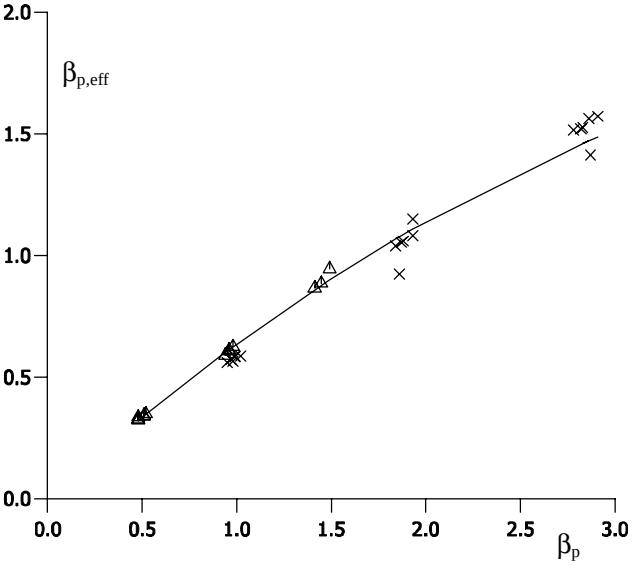

Fig. 5 Computed variation of $\beta_{p,eff}$ with β_p
Δ N=24 , × N=12 , ——— Eq. (5)

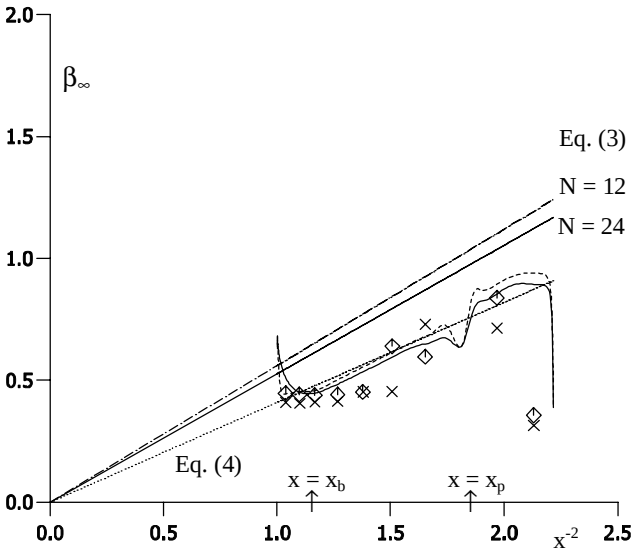

Fig. 6 Computed and measured radial variation of β_∞ for $\beta_p \approx 1$
N = 12, $Re_\phi = 0.75\times10^6$, $\lambda_T = 0.113$, $\beta_p = 1.02$
× measured , ——— computed
N = 24, $Re_\phi = 0.78\times10^6$, $\lambda_T = 0.236$, $\beta_p = 0.98$
◇ measured , ------ computed

Under ideal conditions, the air from the pre-swirl nozzles would flow radially outward creating a free vortex where:

$$\beta_\infty = \beta_p \left(\frac{x_p}{x} \right)^2 \qquad (3)$$

For this system, the free vortex defined by Eq. (3) will have a value of $\beta_\infty = \beta_p$ at $x^{-2} = 1.826$. This "ideal" free vortex is shown, as a straight line passing through the origin, in Figs. 3 and 4.

In fact, *any* straight line passing through the origin in these plots corresponds a free vortex. Due to the momentum losses that occur as the pre-swirl flow mixes with the recirculating flow, the gradient of the actual free vortex will be less than that of the ideal free vortex. It is convenient, therefore, to define an *effective* pre-swirl ratio, $\beta_{p,eff}$, to represent the actual free-vortex flow, such that:

$$\beta_\infty = \beta_{p,eff} \left(\frac{x_p}{x} \right)^2 \qquad (4)$$

where $\beta_{p,eff} < \beta_p$. This "effective free-vortex", based on Eq. (4), is also shown in Figs. 3 and 4. The value of $\beta_{p,eff}$ has been taken as the computed value of β_∞ at $x^{-2} = 1.826$ (where $x = x_p$).

Fig. 3 and Fig. 4 show that the computed distributions of β_∞ follow free vortex behaviour quite closely between the pre-swirl nozzle radius and the receiver outlet radius, $x = x_b$. The computed results shown in Fig. 3 for N = 24 are in reasonably good agreement with the measurements, although the measured values are generally lower than the computed values, suggesting higher mixing losses in the experiments and hence a lower value for $\beta_{p,eff}$. The same comments apply for the results shown in Fig. 4 for N = 12, however there is less good agreement between the computations and measurements for these higher β_p cases.

The difference between $\beta_{p,eff}$ and β_p increases as β_p increases. Fig. 5 shows that the computed variation is represented reasonably well by the following correlation:

$$\frac{\beta_{p,eff}}{\beta_p} = 0.700 - 0.065\beta_p \qquad (5)$$

Karabay et al (2001) also found that a correlation of this form (with different coefficients) described the variation of $\beta_{p,eff}$ with β_p in a simplified cover-plate (rotating cavity) system as described above.

Effect of N on swirl ratio

Fig. 6 shows the computed and measured variation of β_∞ with x^{-2} for $\beta_P \approx 1$, for the two different values of N tested. These results show that the level and distribution of β_∞ is not very sensitive to N at these conditions, although the results for N =12 are slightly lower than those for N = 24, possibly indicating slightly higher mixing losses.

Swirl ratio at the receiver outlet radius

Yan et al (2002) found that the discharge coefficients for the receiver holes depend upon the swirl ratio outside the boundary layers at the receiver outlet radius, $\beta_{\infty,b}$, and correlated the measured variation of $\beta_{\infty,b}$ as follows:

$$N = 12\,(0.9 < \beta_p < 2.9): \quad \beta_{\infty,b} \approx 0.1 + 0.28\beta_p \qquad (6a)$$

$$N = 24\,(0.5 < \beta_p < 1.5): \quad \beta_{\infty,b} \approx 0.1 + 0.34\beta_p \qquad (6b)$$

The present computations were not found to show the same sensitivity to the number of nozzles N. As illustrated in Fig. 3, the computed results for $\beta_{\infty,b}$ for N = 24 are in good agreement with the measurements (and hence with eq. (6b)). Fig. 4 shows that for N = 12 the computed values of $\beta_{\infty,b}$ are higher than the measured values (these computed values were also found to agree with eq. (6b) above).

(Due to the increased computational domain for the N = 12 cases, some grid sensitivity was found for the 99 × 150 × 31 mesh used here for computational economy. Other results, obtained for β_p = 1.86 using a 111 × 199 × 41 grid showed good agreement with the measured value of $\beta_{\infty,b}$.)

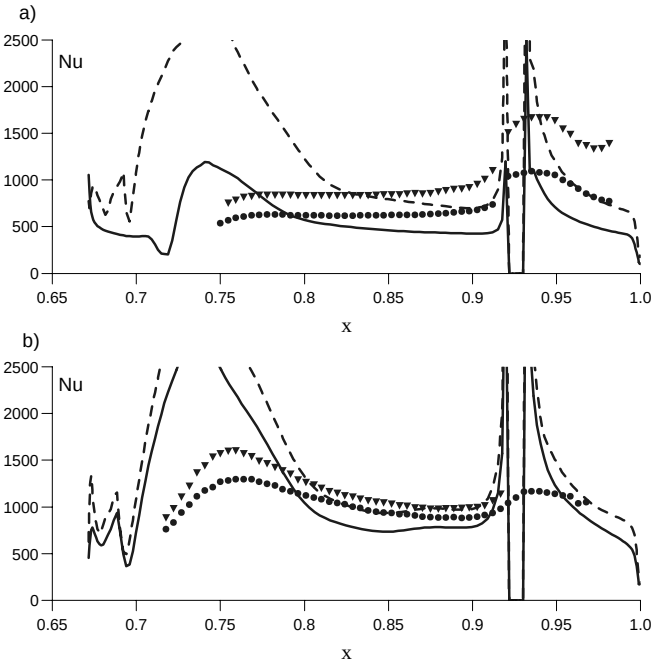

Fig. 7 Effect of Re_ϕ on radial variation of Nu , N = 24

a) $\lambda_T \approx 0.125$, $\beta_p \approx 0.52$; b) $\lambda_T \approx 0.36$, $\beta_p \approx 1.4$

$Re_\phi \approx 0.8 \times 10^6$: ● measured , ——— computed

$Re_\phi \approx 1.2 \times 10^6$: ▼ measured , - - - - - computed

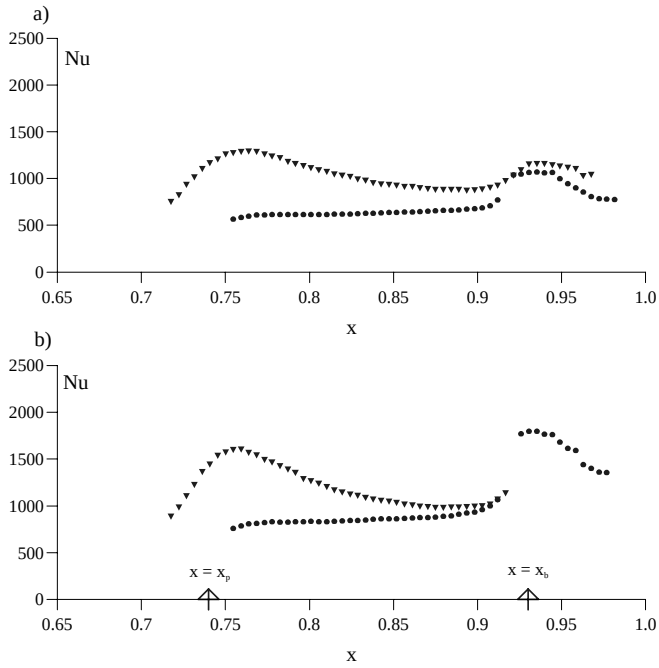

Fig. 8 Effect of λ_T and β_p on measured values of Nu , N = 24

a) $Re_\phi \approx 0.8 \times 10^6$, b) $Re_\phi \approx 1.2 \times 10^6$

● $\lambda_T \approx 0.125$, $\beta_p \approx 0.52$

▼ $\lambda_T \approx 0.36$, $\beta_p \approx 1.4$

HEAT TRANSFER RESULTS

Radial variation of local Nusselt number

Lock et al (2003) presented two-dimensional distributions of measured local Nusselt number for a number of test conditions. These showed nearly axisymmetric behaviour for the heat transfer over the rotating disc surface, except in the regions around and between the receiver holes on the disc. There was generally good repeatability for results obtained between different pairs of holes.

Fig. 7 shows the effect of Re_ϕ on the computed and measured radial variation of Nusselt number at two fixed values of λ_T (0.125 and 0.36 approx.), for which $\beta_P \approx 0.5$ and 1.4 respectively. The measurements correspond to a radial line lying mid-way between receiver holes. For the computational model an annular receiver outlet is used (see Fig. 2), and comparisons with measurements made in the region between holes cannot be made.

For both fixed values of λ_T (and of β_P) shown in Fig. 7, the magnitude of Nu increases with increasing Re_ϕ, but there is little effect of Re_ϕ on the shape of the Nu distributions (for either the computations or the measurements). For all cases, there is a local peak in measured values of Nu in the region near the receiver holes on the disc. Both the measured and the computed results are discussed below.

Referring to the measurements, Fig. 7a ($\lambda_T \approx 0.125$, $\beta_P \approx 0.5$) shows that Nu increases with radius between the pre-swirl nozzle radius, $x_p = 0.74$, and the receiver holes. As discussed by Lock et al, these results suggest that the heat transfer is controlled mainly by the boundary layer flow on the rotating disc. For $x > 0.9$, there is a rapid rise in measured Nu. In this region, disc boundary layer fluid enters the receiver holes and there is strong flow axially toward the disc (see Fig.2), causing an increase in heat transfer.

The computed results for the two $\lambda_T \approx 0.125$, $\beta_P \approx 0.5$ cases shown in Fig. 7a show a large peak in Nu around the pre-swirl nozzle radius, $x_p = 0.74$. This peak results from the use of a low-Reynolds-number, isotropic k - ε turbulence model in a region where anisotropic impinging-flow effects occur near the rotating disc surface (due to the axial component of the pre-swirl flow). Pilbrow et al (1999) found similar behaviour for a different pre-swirl system, and tested an alternative to the Launder-Sharma low-Reynolds-number model used here that gave, in general, a lower peak in the corresponding impingement region. In the present work, there was little difference in results obtained using this alternative model and the Launder-Sharma model.

The computations shown in Fig. 7a mainly underestimate the measured Nusselt numbers for $x_p < x < x_b$, but the computed increase of Nu with increasing Re_ϕ is in reasonable agreement with the measured trend. Modelling simplifications used at the receiver outlet (as described above) may contribute to the large peaks in computed Nu around x = 0.93. Further radially outward, the agreement between computations and measurements is similar to that inward of the receiver holes.

Fig. 7b shows that, for $\lambda_T \approx 0.36$ ($\beta_P \approx 1.4$), a local peak in measured Nu occurs around the inlet nozzle radius x_p, and Nu decreases for $x_p < x < x_b$. This suggests that inertial "impingement" effects, due to the more powerful pre-swirl flow at this higher value of λ_T, have a more significant influence than for the cases shown in Fig. 7a. Fig. 7b shows that computations again reproduce the measured trends reasonably well, although the peak in Nu near $x = x_p$ is greatly exaggerated. There is generally better agreement between the computations and the measurements for the cases shown in Fig. 7b than for those at the lower value of λ_T.

Effect of λ_T and β_P at fixed Re_ϕ

Fig. 8a and Fig. 8b show, respectively, the effect of varying λ_T (and, as a consequence, of varying β_P) on the measured radial variation of Nu for $Re_\phi \approx 0.8 \times 10^6$ and 1.2×10^6. At both values of Re_ϕ, there is a similar transition in the variation of Nu with x, from the viscous behaviour described above for $\lambda_T \approx 0.125$ ($\beta_P \approx 0.5$) to inertial behaviour for the higher values of λ_T (and the corresponding higher values of β_P).

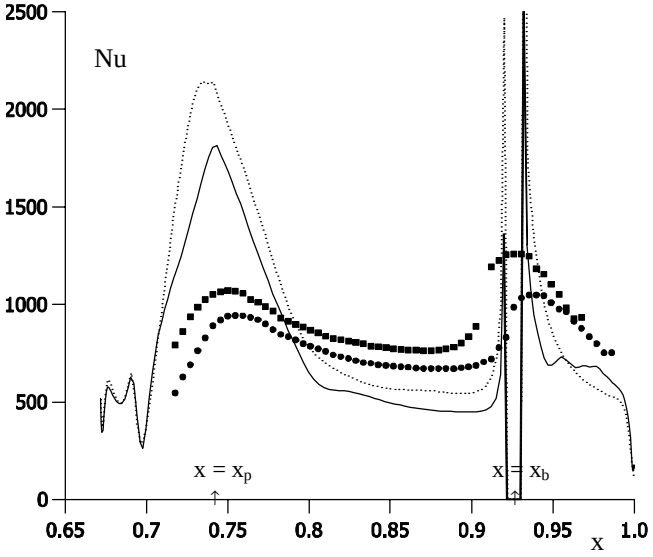

Fig. 9 Computed and measured radial variation of Nu for $\beta_p \approx 1$

N = 12, $Re_\phi = 0.75\times10^6$, $\lambda_T = 0.113$, $\beta_p = 1.02$

● measured , ——— computed

N = 24, $Re_\phi = 0.78\times10^6$, $\lambda_T = 0.236$, $\beta_p = 0.98$

■ measured , ····· computed

The combined effect of increasing λ_T and β_P at fixed Re_ϕ is greatest for $x < 0.9$ approx. Fig. 8 shows that there is less sensitivity to λ_T and β_P for the region around and outward of the receiver holes, and this sensitivity also tends to decrease as Re_ϕ increases. Parametric computations (not shown here) show that Nu increases with both increasing λ_T and increasing β_P when these parameters are varied independently.

Effect of N on heat transfer

For a simple rotating-disc system, heat transfer on the disc is controlled by development of the viscous disc boundary layer, and this is in turn affected by the level of swirl outside the boundary layer, i.e. by β_∞ (Owen and Rogers, 1989).

The results in Fig. 6 show that there is little effect of N on the values of β_∞ for $\beta_P \approx 1$. Fig. 9 shows results for computed and measured Nu for the two cases considered in Fig. 6, These results show that Nu is higher (in both the computations and the experiments) for the N = 24 case than for N = 12. As the level of β_∞ (which influences viscous effects) for these two cases is similar, these results suggest that increased inertial effects, for the higher flow rate at N = 24, are mainly responsible for the increase in Nu. This increase in the magnitude of Nu for N = 24 compared with N = 12 is reproduced reasonably well by the computations, although the measured values are again undepredicted.

CONCLUSIONS

A combined computational and experimental study has been carried out to investigate the effects of flow rate, swirl ratio and rotational Reynolds number on the flow and heat transfer in a pre-swirl rotating-disc system, representative of that found in gas-turbine cooling systems. Measurements of swirl ratio β_∞, and of local Nusselt number Nu on the rotating disc, have been compared with turbulent flow results obtained using a simplified 3D steady computational model of the system.

Computations of β_∞ show that the flow structure follows closely free vortex behaviour for $x_p < x < x_b$. Due to mixing losses that occur between the primary pre-swirl flow and the recirculating secondary flow, this free vortex behaviour corresponds to an effective pre-swirl ratio, $\beta_{P,eff}$, which is lower than the inlet pre-swirl ratio β_P. The difference between $\beta_{P,eff}$ and β_P increases as β_P increases. Measured values of β_∞ were found to be lower than computed values, and there was better agreement between computations and measurements for N = 24 pre-swirl nozzles (for which $\beta_P < 1.5$) than for higher values of β_P obtained using N = 12.

Measurements and computations of heat transfer both show that values of Nu increase as Re_ϕ, λ_T and β_P increase. The measurements suggest that heat transfer is controlled by viscous effects at low values of λ_T, and by inertial effects at high values of λ_T . Measured values of Nu were mainly underpredicted, except in the region around the pre-swirl nozzle radius where inertial "impingement" effects are predicted poorly by the low-Reynolds-number k-ε turbulence model used.

ACKNOWLEDGMENTS

The experimental work was funded by Alstom Power Ltd and the UK EPSRC. The computations were carried out as part of PhD research supported by the Iranian government.

REFERENCES

Karabay, H., Wilson, M. and Owen, J. M., 2001, Predictions of effect of swirl on flow and heat transfer in a rotating cavity, *Int. J. Heat and Fluid Flow*, v. 22, pp 143-155

Launder, B. E. and Sharma, B. I., 1974, Application of the energy-dissipation model of turbulence to flow near a spinning disc, *Letters in Heat and Mass Transfer*, 1974, v. 1, pp 131-138

Lock, G. D., Yan, Y., Newton, P. J., Wilson, M. and Owen, J. M., 2003, Heat transfer measurements using liquid crystal in a pre-swirl rotating-disc system, ASME paper GT-2003-38123

Owen, J. M. and Rogers, R. H., 1989, Flow and heat transfer in rotating disc systems: Vol. 1, Rotor-stator systems, Research Studies Press, Taunton, UK and John Wiley, NY

Owen, J. M. and Wilson, M., 2000, Some current research in rotating-disc systems, Turbine 2000 Int. Symp. on Heat Transfer in Gas Turbine Systems, Turkey, August 13-18, in Heat Transfer in Gas Turbine Systems, Annals of the New York Academy of Sciences, v 934, pp 206-221

Pilbrow, R., Karabay, H., Wilson, M. and Owen, J. M., 1999, Heat transfer in a "cover-plate" pre-swirl rotating-disc system, *J. Turbomachinery*, v. 121, pp 249-256

Yan, Y., Farzaneh-Gord, M., Lock, G. D., Wilson, M. and Owen, J. M., 2002, Fluid dynamics of a pre-swirl rotor-stator system, ASME paper GT-2002-30415 (to be published in Trans ASME)